Supporting Information

Zhang *et al.* 10.1073/pnas.0708583105

SI Text

Determination of Equilibrium Binding Constants from Sedimentation Velocity Data. Sedimentation of a low-molecular weight peptide in the presence of either tSH2 or $tSH2_{pm}$ was monitored by following the absorbance maximum of the fluorophore 5-carboxyfluorescein N-terminally linked to dp-ITAM. Sedimentation of tSH2 was detected simultaneously from the interferograms. The fraction of bound peptide as a function of total peptide concentration was calculated from the integrated area of the slowly sedimenting species ($s \sim 1$ S) and the one sedimenting with tSH2 ($s \sim 2.5$ S) in the concentration distribution plot. Equilibrium binding constants for dp-ITAM associating with different Syk constructs were determined using a final peptide concentration ranging from 1 μM to 10 μM. The concentration of 5′-carboxyfluorescein-dp-ITAM peptide was determined from 490-nm absorbance and the concentration of protein from interference fringe displacement. Binding data from five runs were fit to the following equation using the program Origin to estimate K_D:

$$[\text{tSH2}\cdot\text{ITAM}]^2 - \{[\text{tSH2}]_{\text{total}} + [\text{ITAM}]_{\text{total}} - K_D\}^* [\text{tSH2}\cdot\text{ITAM}] + [\text{tSH2}]_{\text{total}}{}^*[\text{ITAM}]_{\text{total}} = 0. \quad [1]$$

The binding curve is shown in Fig. S1.

Relaxation Data Analysis. Relaxation rates measured at 600 MHz were extracted for 97 residues of Syk tSH2 and 134 residues of $tSH2_{pm}$. Residue values for R_1 and R_2 are plotted in Figs. S2–5S. The residues corresponded to ^{15}N-HSQC resonances having NOEs >0.65, R_2/R_1 values within one standard deviation of the average and residues within secondary structure elements (1). R_1, R_2, and NOE values were measured in duplicate. Average values for each residue, $\langle R_1 \rangle$ and $\langle R_2 \rangle$, were used to calculate R_2/R_1. The percentage error in R_2/R_1 reported in Table 1, main text, is the average of the residue values for their propogation of error. The propogation of error for each residue is: $\sqrt{(\sigma_{R2}/\langle R_2 \rangle)^2 + (\sigma_{R1}/\langle R_1 \rangle)^2}$, where σ is the standard deviation over duplicate experiments for that residue.

Correlation times and rotational diffusion tensor elements were determined from R_1, R_2, and crystallographic coordinates using the program TENSOR2.0 and from crystallographic coordinates using HYDRONMR (Table 1S). The NMR relaxation data for Syk tSH2 are in good agreement with the Syk tSH2 (ITAM-bound) crystal structure (PDB entry 1A81), residues 9–262. There are six molecules in the crystallographic asymmetric unit of 1A81, and these vary in the relative orientation of the two SH2 domains by as much as 18°. Values predicted from these molecules differ by <1 ns for τ_c, and R_2/R_1 average values exhibit a range of 3.5. The τ_c analysis shows that introduction of negative charge at Y130 acts to partially decouple the SH2 domains by altering the 45-residue interdomain A conformation in a manner that enhances flexibility but retains sufficient compactness to restrain SH2 domain rotation. Restriction by a linker on rotational tumbling of adjacent, structured regions was observed for another protein (2).

RDC Data Analysis, Relative SH2 Domain Orientation. Five hundred Monte Carlo simulations were used to assess the validity of the anisotropic models using the MATLAB-based program RDCA (3) and an input molecular structure. Alignment parameters were fit to the RDC values measured for 55 tSH2 residues (29 N-SH2 plus 26 C-SH2 residues) and 98 $tSH2_{pm}$ residues (48 N-SH2 plus 50 C-SH2 residues). RDC values were measured for 15 residues in interdomain A but not used in any model fitting.

RDCs, which depend on angular orientation of the N-H bond vector in the molecular alignment frame, were fit for a given domain to a crystallographic model by varying the alignment tensor parameters to minimize differences in observed and calculated RDCs. The Euler angles (α, β, and γ) for conversion of the alignment frame to the crystallographic coordinate frame, along with the axial (Aa) and rhombic (R) components of the alignment tensor, were determined by independent optimization of RDCs from either N-SH2 or C-SH2 (Table S2), or by optimization for the full tSH2 structure (n + C). Experimental data for tSH2 and $tSH2_{pm}$ were fit to crystallographic coordinates for ITAM-bound Syk tSH2 (PDB entry 1A81) and for unligated Zap-70 tSH2 (PDB entry 1M61). These two structures differ in the relative orientation of the two SH2 domains by ≈50°.

We observe from the RDC analysis of independently fitting the two SH2 domains that both SH2 domains of Syk tSH2 are fit to 1A81 with approximately the same alignment parameter values while much larger differences in the values, particularly A_a, are obtained for all other cases of independently fitting N- and C-SH2 RDC data to crystallographic coordinates. In the case of fitting the overall tSH2 structure (n + C), the quality of the fit is worse, particularly in the case of $tSH2_{pm}$, again illustrating the change in domain orientation between tSH2 and $tSH2_{pm}$. Further, the SH2-SH2 domain orientation of Syk tSH2 in solution agrees well (as determined from RDCs) with the crystal structure of ITAM-bound Syk tSH2, but not with that of unligated Zap-70 tSH2. The solution orientation for $tSH2_{pm}$ (tSH2 phosphorylation mimic with negative charge at position 130) agrees with neither the SH2-SH2 orientation of ITAM-bound Syk tSH2 nor that of unligated Zap-70 tSH2.

Analytical Ultracentrifugation. Protein samples were loaded into double-sector, charcoal-filled Epon centerpieces, placed in an An60 Ti four-hole rotor, and mounted to a Beckman Coulter XL-I analytical ultracentrifuge equipped with UV-Vis absorbance and Rayleigh interference optical systems. The samples were subjected to sedimentation at 50,000 rpm for 8 h at 20°C. Sedimentation coefficients were extracted from the Lamm equation using the program SEDFIT (4). Experimental s values were corrected for buffer conditions and protein concentration to obtain $s_{20,w}$. The data were analyzed by SEDNTERP using both the v-bar and Teller methods. The degree of asymmetry and degree of hydration were estimated from s/s_{max} values, and axial ratios have been estimated assuming an oblate ellipsoid molecular shape indicated by ^{15}N relaxation. Single sedimenting species were observed for both tSH2 and $tSH2_{pm}$. The apparent molecular weight for each construct was consistent with the theoretical value, indicating that both proteins exist as homogenous monomers in solution.

Syk Tandem SH2 Structure Tolerates Substitution at Position Y130 in Linker A. Results obtained for the variant Y130F show that the overall structure of the tandem SH2 is stable to substitution at position 130. An overlay of ^{15}N HSQC spectrum of the variant Y130F of tSH2 and wild-type tSH2 (Fig. 6S) shows no significant difference.

Materials. $^{15}NH_4Cl$ was purchased from Spectra Gases; D-glucose (U-^{13}C6, 99%, 1, 2, 3, 4, 5, 6, 6-D7, 98%) and 99% deuterium oxide were purchased from Cambridge Isotope Laboratories. Fluorescently labeled Igα-dpITAM peptide (5-FAM-ENL-pY-EGLNLDDCSM-pY-EDISR-CONH2) was obtained from Syn-Pep. N-terminally biotinylated dp-ITAM peptide was synthesized by a Purdue Cancer Center facility. Streptavidin-agarose was obtained from Sigma. Anti-Syk (N19) antibodies were obtained from Santa Cruz Biotechnology.

Sample Preparation. cDNA for wild-type murine Syk tandem SH2 domain (tSH2) Ser-9-Gln-265 was cloned into vector pET-30a(+) (Novagen) and expressed in *Escherichia coli* strain BL21(DE3). ^{15}N-^{13}C-^{2}H labeled tSH2 was purified by affinity chromatography on phosphotyrosine-agarose, concentrated to 0.7–1 mM in sodium phosphate buffer at pH 7.5 and stored at 4°C. The sample was >95% homogenous based on SDS/PAGE analysis. $tSH2_{pm}$ was constructed using the QuikChange™ Site-Directed Mutagenesis Kit (Stratagene) to replace Y130 with E130 and purified as described above.

NMR Data Collection. All NMR spectra were recorded at 20°C on a Varian Unity *plus* 600-MHz spectrometer, processed using NMRPipe (5) and analyzed with SPARKY3.106 (6). ^{2}H-decoupled, TROSY-based 3D HNCA, HN(CO)CA, HNCACA, HN(CO-CA)CB experiments were performed on tSH2 and $tSH2_{pm}$ 0.7–1.0 mM samples, and H_N, N, C_α, and C_β were assigned using the program MARS (7). Backbone amide ^{15}N relaxation measurements were acquired with T_1/T_2 options enabled in gNhsqc pulse sequence from BioPack. The ^{15}N- (8) NOE spectrum was recorded with 3-s proton saturation after 3-s recycling time; for the unsaturated reference spectrum, a 6-s recycle delay was used.

To measure residual dipolar coupling constants, the protein was mixed with a final concentration of 10 mg/ml filamentous phage Pf1 (9). The in-phase anti-phase (IPAP) pulse scheme was used to measure the coupling constants in the nitrogen dimension of an ^{1}H-^{15}N HSQC spectrum (10).

1. Dosset P, Hus JC, Blackledge M, Marion D (2000) Efficient analysis of macromolecular rotational diffusion from heteronuclear relaxation data. *J Biomol NMR* 16:23–28.
2. Zhou H, *et al.* (1996) Phosphotransfer and CheY-binding domains of the histidine autokinase CheA are joined by a flexible linker. *Biochemistry* 35:433–443.
3. Skrynnikov NR, *et al.* (2000) Orienting domains in proteins using dipolar couplings measured by liquid-state NMR: Differences in solution and crystal forms of maltodextrin binding protein loaded with beta-cyclodextrin. *J Mol Biol* 295:1265–1273.
4. Schuck P (2000) Size-distribution analysis of macromolecules by sedimentation velocity ultracentrifugation and lamm equation modeling. *Biophys J* 78:1606–1619.
5. Delaglio F, *et al.* (1995) NMRPipe: A multidimensional spectral processing system based on UNIX pipes. *J Biomol NMR* 6:277–293.
6. Goddard TD, Kneller DG (2008) SPARKY 3 (University of California, San Francisco).
7. Jung YS, Zweckstetter M (2004) Mars–robust automatic backbone assignment of proteins. *J Biomol NMR* 30:11–23.
8. Buchko GW, McAteer K, Wallace SS, Kennedy MA (2005) Solution-state NMR investigation of DNA binding interactions in Escherichia coli formamidopyrimidine-DNA glycosylase (Fpg): A dynamic description of the DNA/protein interface. *DNA Repair* (*Amst*) 4:327–339.
9. Hansen MR, Mueller L, Pardi A (1998) Tunable alignment of macromolecules by filamentous phage yields dipolar coupling interactions. *Nat Struct Biol* 5:1065–1074.
10. Ottiger M, Delaglio F, Bax A (1998) Measurement of J and dipolar couplings from simplified two-dimensional NMR spectra. *J Magn Reson* 131:373–378.
11. Garcia de la Torre J, Huertas ML, Carrasco B (2000) HYDRONMR: Prediction of NMR relaxation of globular proteins from atomic-level structures and hydrodynamic calculations. *J Magn Reson* 147:138–146.

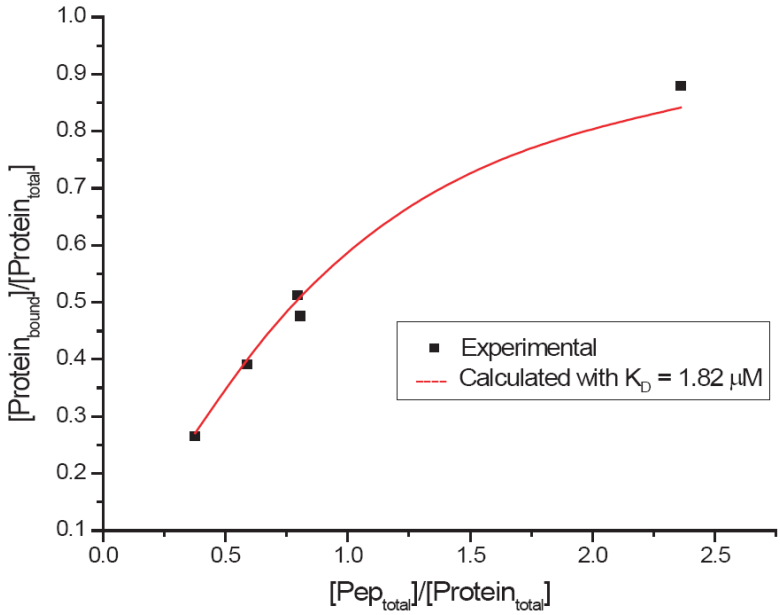

Fig. S1. Binding curve from sedimentation velocity experiments for Syk $tSH2_{pm}$ in the presence of 5′-carboxyfluorescein-dp-ITAM. Experimental points were estimated as described in *Determination of Equilibrium Binding Constants from Sedimentation Velocity Data*.

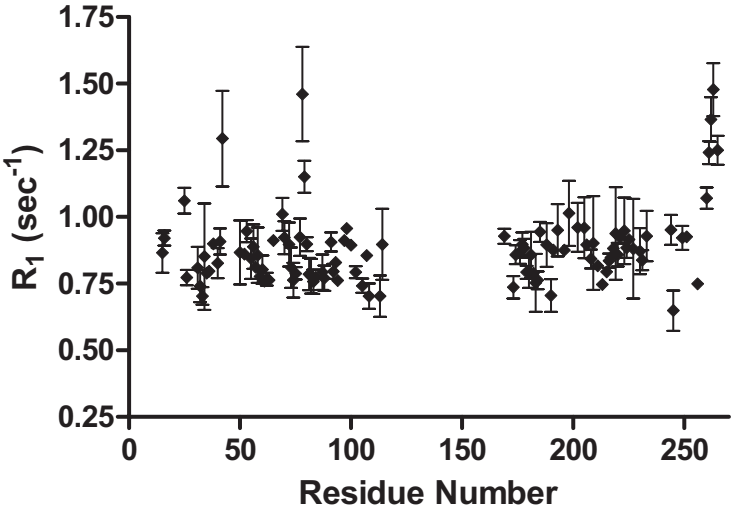

Fig. S2. tSH2 R_1 values with error bars plotted as a function of residue number.

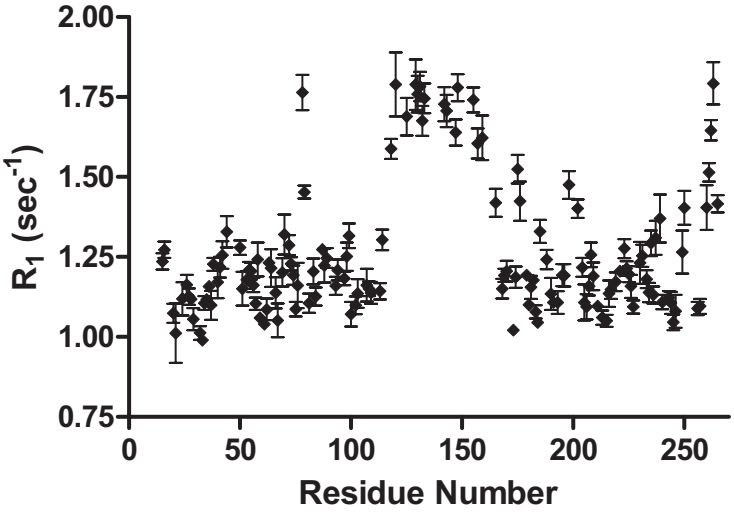

Fig. S3. tSH2$_{pm}$ R_1 values with error bars plotted as a function of residue number.

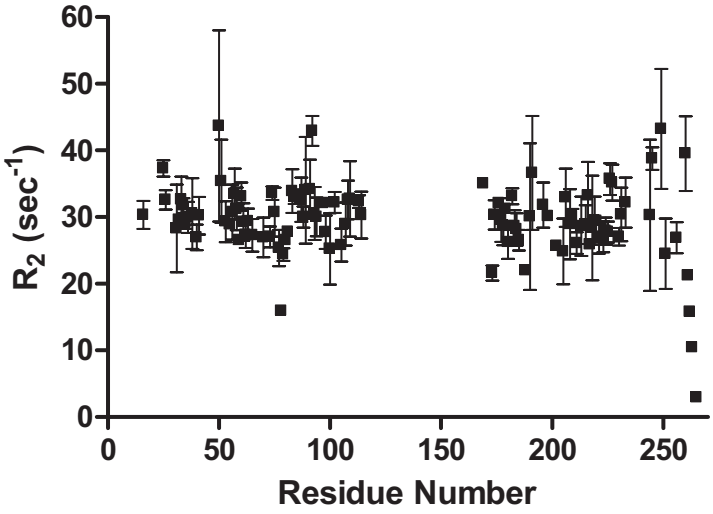

Fig. S4. tSH2 R_2 values with error bars plotted as a function of residue number.

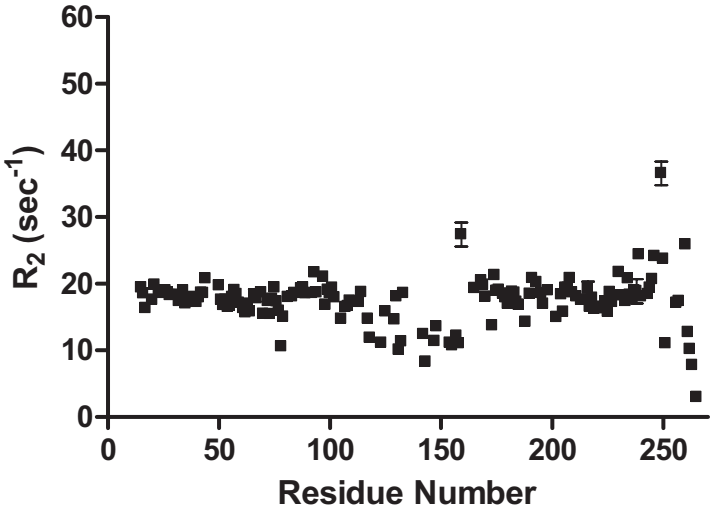

Fig. S5. tSH2$_{pm}$ R_2 values with error bars plotted as a function of residue number.

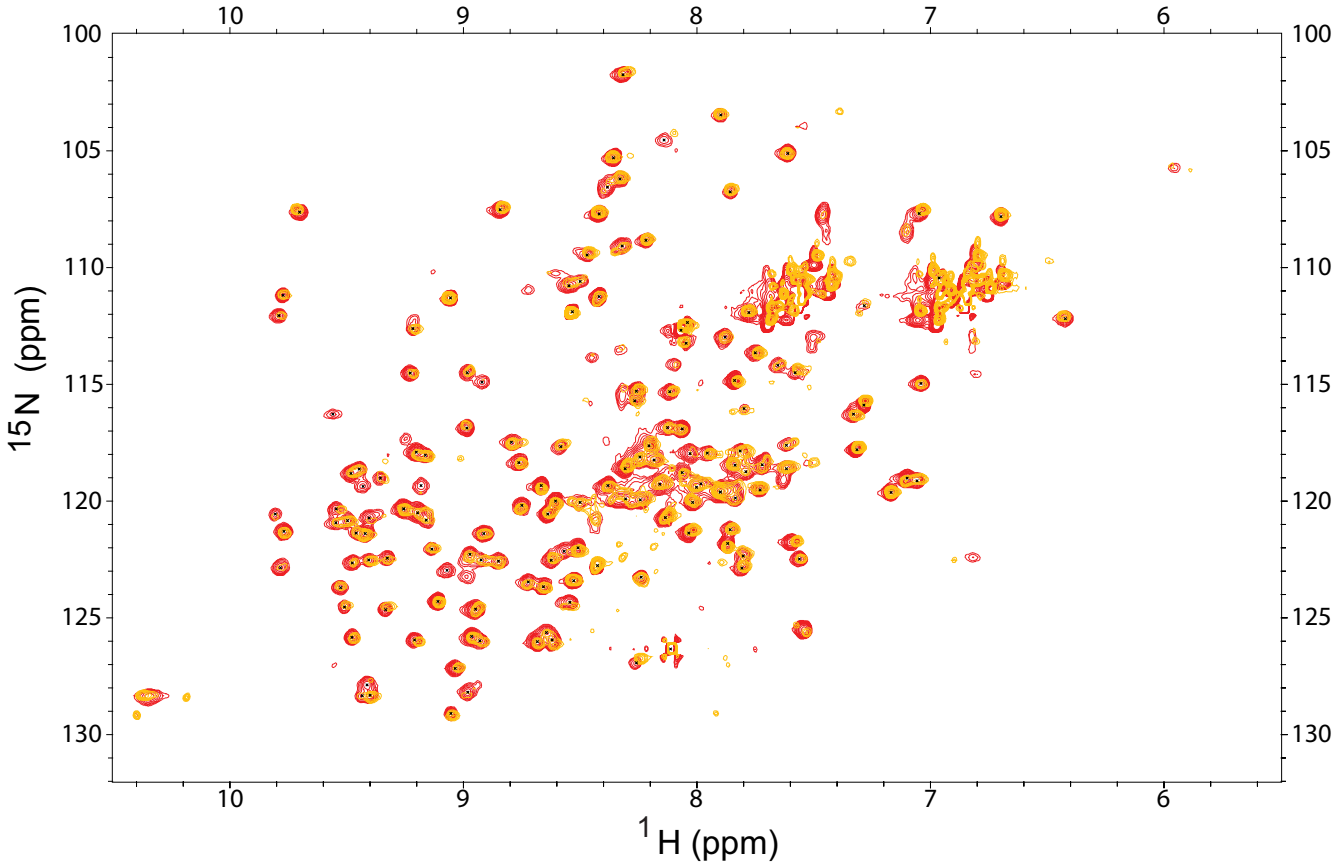

Fig. S6. ^{15}N-HSQC spectra of wild-type Syk tSH2 (red) overlayed with the variant Syk Y130F tSH2 (yellow) recorded at 600 MHz, 20°C.

Table S1. Comparison of the diffusion tensor calculated from experimental heteronuclear relaxation (measured at 600 MHz, 293 K) and estimates calculated from structure coordinates

R_2/R_1	Crystal coordinates	τ_c, ns	D_{xx} or D_2, 10^6 s^{-1}	D_{yy},* 10^6 s^{-1}	D_{zz} or $D_\perp$, 10^6 s^{-1}
tSH2, NMR	1A81 Res 2–262	19.2	7.16		9.54
Predicted†	1A81 Res 2–262	19.5	7.19	8.68	9.79
$tSH2_{pm}$ (N-SH_2), NMR	1A81 Res 9–114	12.2	12.3		14.4
$tSH2_{pm}$ (C-SH_2), NMR	1A81 Res 160–262	12.2	12.0	14.2	15.0

Res, residues. R_2/R_1 measurements and crystal coordinates were input to TENSOR2 to determine τ_c and rotational diffusion tensor components. Crystal coordinates were input to HYDRONMR (11) to estimate from the PDB (Syk tSH2, ITAM-bound; PDB entry 1A81) R_2, R_1, τ_c, and rotational diffusion tensor components (radius of the atomic elements, a = 2.5 Å, 293 K).

*If no value is shown for D_{yy}, then an axial symmetric model was fit.

†Predicted by HYDRONMR.

Table S2. Alignment parameters determined from RDC values measured for tSH2 and $tSH2_{pm}$

Molecule	Domain	α,* °	β,* °	γ,* °	Aa†	R‡	R_{dip}‡
Syk tSH2, ITAM-bound; PDB entry 1A81							
tSH2	N-SH2	80	65	140	−0.00166	0.39	0.37
	C-SH2	75	82	131	−0.00161	0.59	0.29
	N + C	74	82	131	−0.00164	0.46	0.47
$tSH2_{pm}$	N-SH2	92	49	133	0.00120	0.38	0.34
	C-SH2	6	31	15	−0.000884	0.44	0.28
	N + C	100	83	117	0.00086	0.59	0.61
Zap-70 tSH2, unligated; PDB entry 1M61							
tSH2	N-SH2	157.5	86.7	170.0	−0.00153	0.53	
	C-SH2	103.1	111.4	128.5	0.00154	0.16	
$tSH2_{pm}$	N-SH2	153.1	58.4	349.2	0.00124	0.37	
	C-SH2	124.1	107.6	176.6	−0.000932	0.31	

Alignment parameters were estimated using the program RDCA (3) by independently fitting the measured RDCs of the N-SH2 and C-SH2 domains to crystallographic coordinates (tSH2 and $tSH2_{pm}$) or simultaneous fit of both SH2 domains (tSH2). The two crystallographic structures, 1A81 (Syk tSH2, ITAM-bound) and 1M61 (Zap-70 tSH2, unligated), differ in the relative orientation of N-SH2 and C-SH2 by approximately 50°.

*α, β, and γ are Euler angles for the conversion of the alignment tensor frame into the molecular frame.

†A_a and R are the unitless axial and rhombic components of the alignment tensor.

‡Quality factor of the fit of RDC values calculated from structure, D^{calc}, to the measured RDC, D^{meas}, [GRAPHIC].